Theoretical study of elastic electron scattering by zinc atoms in the framework of relativistic optical potential model

Vladimir I Kelemen, Sándor Demes, Eugene Yu Remeta

Journal of Electron Spectroscopy and Related Phenomena 266 (2023) 147365

Contents lists available at ScienceDirect

Journal of Electron Spectroscopy and Related Phenomena

journal homepage: www.elsevier.com/locate/elspec

Theoretical study of elastic electron scattering by zinc atoms in the framework of relativistic optical potential model

Vladimir I. Kelemen [a], Sándor Demes [b,*], Eugene Yu. Remeta [a]

[a] Institute of Electron Physics, Universitetska str. 21, 88017 Uzhhorod, Ukraine
[b] Institute for Nuclear Research (ATOMKI), Bem square 18/c, 4026 Debrecen, Hungary

ARTICLE INFO

Keywords:
Elastic scattering
Optical potential
Shape resonance
Critical minima
Total polarization points
Sherman function

ABSTRACT

A theoretical study of integral and differential cross sections as well as of spin-polarization effects is reported for elastic electron scattering by zinc atoms at collision energies up to 3 keV. It has been shown that a *P*-wave shape resonance appears in the low-energy range of the integral cross sections. Its energy is about 0.19 and 0.20 eV, while its width is about 0.309 and 0.356 eV for the $j = 3/2$ and $j = 1/2$ total angular momentum of the electron, respectively. The differential cross sections of scattering and the Sherman-functions $S(E, \theta)$ are computed by the parameter-free complex optical potential method. The calculated data are in a good overall agreement with the available experimental and theoretical data in the literature. The energy and angular positions have been located for five critical minima in the differential cross sections. The low-energy minimum is located at [6.63 eV; 102.34°], while the high-energy minimum is at [347.53 eV; 124.11°]. Ten points for the scattered electrons' total spin-polarization ($S = \pm 1$) have been found in the vicinity of the critical minima along with the energy and the angular widths of the spin-polarization peaks (where $|S| \geq 0.9$).

1. Introduction

The zinc atom, along with Cd and Hg atoms, belongs to the IIB group of the Periodic Table and is characterized with mono-electronic sub-valence configurations – [core]$(n\text{-}1)d^{10}ns^2$, where [core] = [Ar], [Kr], [Xe4f^{14}] and $n = 4$, 5, 6. Due to their properties, the elements of this subgroup are used in various fields of technology, for instance in modeling the physical processes of low-temperature plasma, in solid-state and surface physics, *etc*.

The differential (DCSs) and integral cross sections (ICSs) of elastic electron scattering by zinc atoms have been recently measured [1] at energies between 10 and 100 eV. DCS data have been obtained in the angular range of 10–150° with an angular step of 5° and 10°. The measured values are in a good agreement with the results of different theoretical methods, including the optical potential (OP), *B*-spline R-matrix (BSR) [2] and convergent close coupling (CCC) [3] models. The authors of work [1] have used the non-relativistic (NOP) and relativistic (ROP) optical potential model for their calculations (see the details in Ref(s). [5] and [1]). In both these approaches, the optical potential contains the static, exchange, polarization and absorption terms, however the absorption effects significantly differ in the two cases.

The recommended theoretical values for elastic, inelastic (total cross sections of discrete excitation and ionization) as well as momentum transfer cross sections are discussed in work [4]. These scattering data are computed for a broad range of energies (0.01–5000 eV) using the non-relativistic and relativistic optical potential approaches [5] (see also [4]). It is worth to mention that the low-energy behavior of elastic electron scattering by zinc atoms (e^- + Zn) is poorly investigated and theoretical studies are important for these processes. The nature of the minima along the DCS also requires more research, with the aims to find which of them can be treated as critical minima (CM) and also to investigate the spin-polarization of electrons inside and in the vicinity of these minima.

The studies [6,7] are devoted to calculate the properties of the CM in order to compare with experiment [8] for DCS minima. The e^- + Zn elastic scattering is studied from 10 up to 40 eV energies in the relativistic approximation of the polarized orbitals method with a frozen core approach. This model is based on the Dirac-Fock equations with exact exchange and model polarization potentials, but without taking into account the absorption effects. The elastic cross sections in [9] are calculated for e^- + Zn and e^- + Cd scattering by the optical potential

* Corresponding author.
E-mail address: demes.sandor@atomki.hu (S. Demes).

https://doi.org/10.1016/j.elspec.2023.147365
Received 3 May 2023; Received in revised form 21 June 2023; Accepted 22 June 2023
Available online 28 June 2023

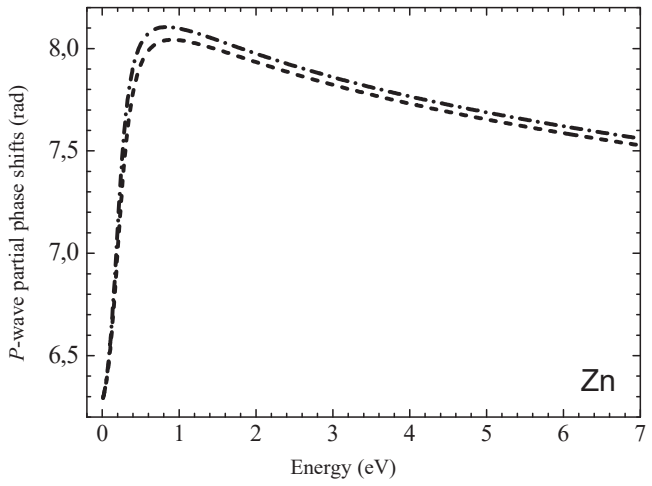

Fig. 1. Energy dependence of the *P*-wave partial phase shifts for elastic e^- + Zn scattering (in radians). RSEP theory: dash-dot line – $\delta^- = \delta(j = 1/2)$, dashed line – $\delta^+ = \delta(j = 3/2)$.

Table 1
Energy (E_r) and width (Γ) of the P-wave shape resonance as well as the energy position of the maximum (E_{max}) in the *P*-wave partial cross section of the e^- + Zn scattering.

Method	E_r (eV)		Γ(eV)		E_{max}(eV)
	$j = 3/2$	$j = 1/2$	$j = 3/2$	$j = 1/2$	
Present with MFM	0.19	0.2	0.309	0.356	**0.28**
Present with FM	0.066	0.044	0.057	0.029	0.07
Present with FEG	0.43	0.43	1.59	1.51	0.9
Present ELSEPA	–	–	–	–	0.3
[1]			–		0.4 (NOP); 0.3 (ROP)
[2]			–		0.71
Exper.[36]			–		0.49

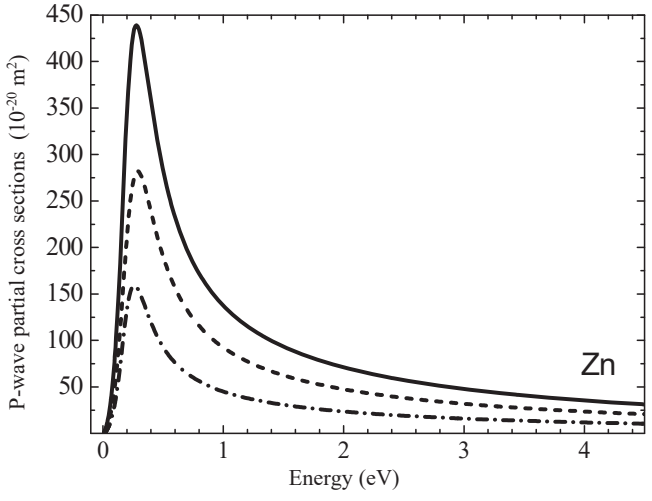

Fig. 2. Energy dependence of the *P*-wave partial cross sections for elastic e^- + Zn scattering (in units of 10^{-20} m^2). RSEP theory: dash-dot line – $\sigma_{1/2}$, dashed line – $\sigma_{3/2}$, solid line – $\sigma = \sigma_{3/2} + \sigma_{1/2}$.

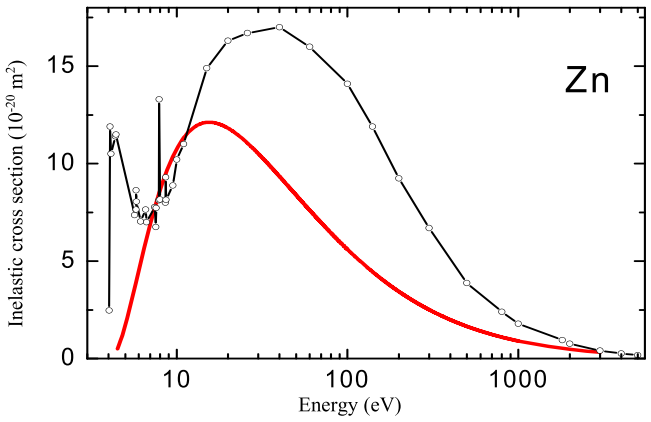

Fig. 3. Energy dependence of the inelastic integral cross section σ_{abs} (see Eq. (19)) for e^- + Zn scattering (in units of 10^{-20} m^2). Theory: red solid line – RSEPA calculations with absorption potential VaMc; black line with circles – recommended data from Ref. [4].

Table 2
The values of the $W(E)$ parameter (in a.u.) as used in the absorption potential VaMc to calculate the e^- + Zn scattering parameters.

E(eV)	$W(E)$	E(eV)	$W(E)$	E(eV)	$W(E)$
5	0.008926	80	19.060	500	390.02
8	0.13372	100	27.833	600	522.29
10	0.28142	125	40.468	700	667.36
15	0.81090	150	54.790	800	824.42
20	1.5149	200	88.027	900	993.03
30	3.3435	250	126.85	1000	1172.27
40	5.6654	300	170.80	2000	3440.10
50	8.4310	350	219.42	2500	4847.00
60	11.606	400	272.26	3000	6412.67

model, including the static, polarization and exchange (Furness-McCarthy) terms. Collision energies from 12.5 to 200 eV are considered.

In the vicinity of the deepest minimum (i.e. the so-called critical minimum) of an 'electron' + 'atom' DCS, the scattered electron's total spin-polarization can be derived [10]. It is important to note however that such specific scattering properties like the CM and the spin-polarization parameters are good probes of both the experimental as well as the theoretical methods. The properties of the CM in elastic electron scattering by mercury atoms (which is the last element of subgroup IIB, where zinc belongs too) have been studied in our previous work [11].

In the present paper, we study the general behavior and the specific features of the integral (resonances) and differential (minima) cross sections as well as of the spin-polarization (Sherman functions, Total Polarization Points) in e^- + Zn elastic electron scattering, using the relativistic OP approximation. A broad collision energy range is explored, from 0.01 up to 3000 eV. In addition, we compare the calculated cross sections using our approach with those of obtained by the ELSEPA code [12]. The relativistic effects have been taken into account by implementing into the OP the spin-orbit interaction [13] and the scalar part of Dirac's relativistic potential [14]. The different terms in the interaction potential for the 'incident electron' + 'target atom' system are usually defined by the total and valence electron densities of the target atom. These densities and the corresponding atomic properties are calculated in the local approximation of the density functional theory (DFT), with relativistic effects taken into account. Therefore, the description of the scattering process in our OP approximation is consistent with the description of the atom to a certain extent. The results of our calculations for DCSs, ICSs and Sherman functions are compared with the available experimental and theoretical data.

The elastic, momentum transfer and viscosity integral cross sections

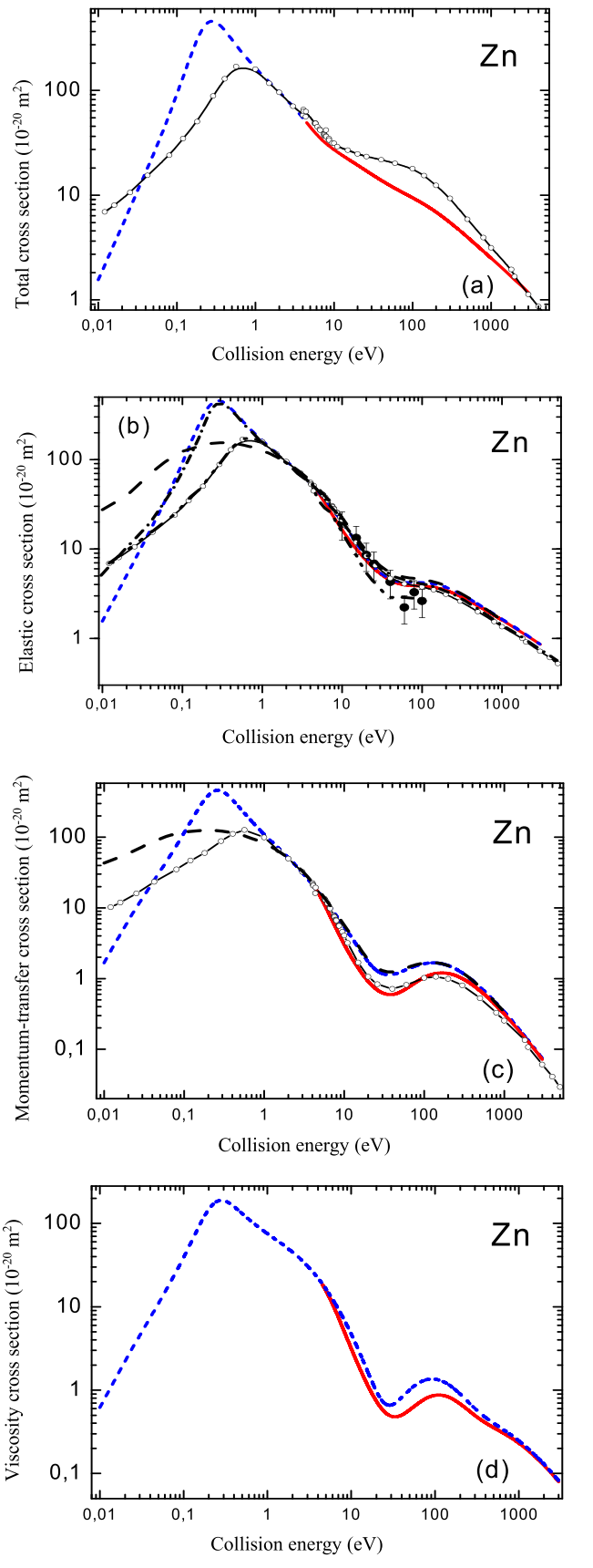

(caption on next column)

Fig. 4. Energy dependence of the total $\sigma_{tot}(E)$ (23) (a), elastic $\sigma_{e\ell}(E)$ (18) (b), momentum-transfer $\sigma_{mom}(E)$ (20) (c) and viscosity $\sigma_{vis}(E)$ (21) (d) integral cross sections for e^- + Zn scattering (in units of 10^{-20} m^2). Theory: red solid lines – RSEPA calculations with absorption potential VaMc; blue dashed lines – RSEP calculations; black long dashed lines – calculations by ELSEPA; black dash-dotted lines – ROP calculations [1]; black dash-dot-dotted lines – BSR-36 calculations [2]. • – experimental data [1]. Black line with circles – recommended data from Ref. [4].

are important observables in electron-atom collisions. For instance, the cross sections are widely used in solid-state physics as well as in surface physics studies. They have also particular applied interest in experimental methods with electron beams as well as in structural analysis for material science. The properties of the angular and energy dependence of the cross sections and even the scattering phase shifts could be used in various applications. Therefore, the need to obtain reliable and detailed collisional data for 'electron' + 'atom' scattering is an important stimulus for their further refining.

From the perspective of a theoretical study, zinc is a many-electron atom which requires the inclusion of relativistic and correlation effects in its scattering studies. The spin-polarization parameters $S(\theta)$, $T(\theta)$, $U(\theta)$ are more sensible scattering properties than the cross sections (for example, see [15]). The angular and energy dependence of these parameters are derived from the direct and spin-flip scattering amplitudes, both of which have a real and an imaginary part. Their specific features (i.e. the deep, narrow minima or the large maxima) are related to the scattered electron's total spin-polarization, which is determined by the properties of the CM in the differential scattering cross sections.

Following the review of the existing theoretical studies one can see that, despite the fact they adequately treat the DCSs and spin-polarization parameters, they do not provide however a detailed description about the cross section minima, and in particular – about the CM. There are also no data available for the extreme behavior of the spin-polarization parameters in the vicinity of the CM.

2. Calculation method

We will recall hereinafter the studies of the scattering process in the relativistic complex OP approach within the RSEPA-approximation, where

$$V^{\pm}_{opt}(r,E) = V^{\pm}_{R}(r,E) + iV_A(r,E)\ . \tag{1}$$

The scattering properties could be also calculated without taking into account the absorption potential $V_A(r, E)$, i.e. using exclusively the parameter-free, real part of the OP (this is the so-called RSEP-approximation):

$$V^{\pm}_{R}(r,E) = V_{st}(r) + V_e(r,E) + V_p(r) + V^{\pm}_{so}(r,E) + VRS(r,E)\ . \tag{2}$$

The terms V_{st}, V_e and V_p in (2) are the static, exchange and polarization potentials, respectively. The spin-orbit interaction potential $V^{\pm}_{so}$ and the scalar part of the Dirac-type potential $VRS(r, E)$ are used in order to take into account the relativistic effects of the scattering. The "± " sign corresponds to the value of the total angular momentum of the electron $j = \ell \pm 1/2$, ℓ being the orbital angular momentum. Throughout the paper we use atomic units (a.u.): $\hbar = e = m_e = 1$, $E = k^2/2$ is the incident electron's energy, k is the incident electron's momentum.

The static potential $V_{st}(r)$ is related to the total electron density $\rho(r)$ of the Zn atom and they are calculated from analytical expressions (see (A1) and (A2) in Appendix A) [16]. The parameters in these expressions and in the formula for valence density $\rho_{4s}(r)$ (see (B.1), (B.2) in Appendix B) were obtained by the best fit to the initial density tables.

The spin-orbit interaction of the incident electron with the target atom has been taken into account using the following potential [13]:

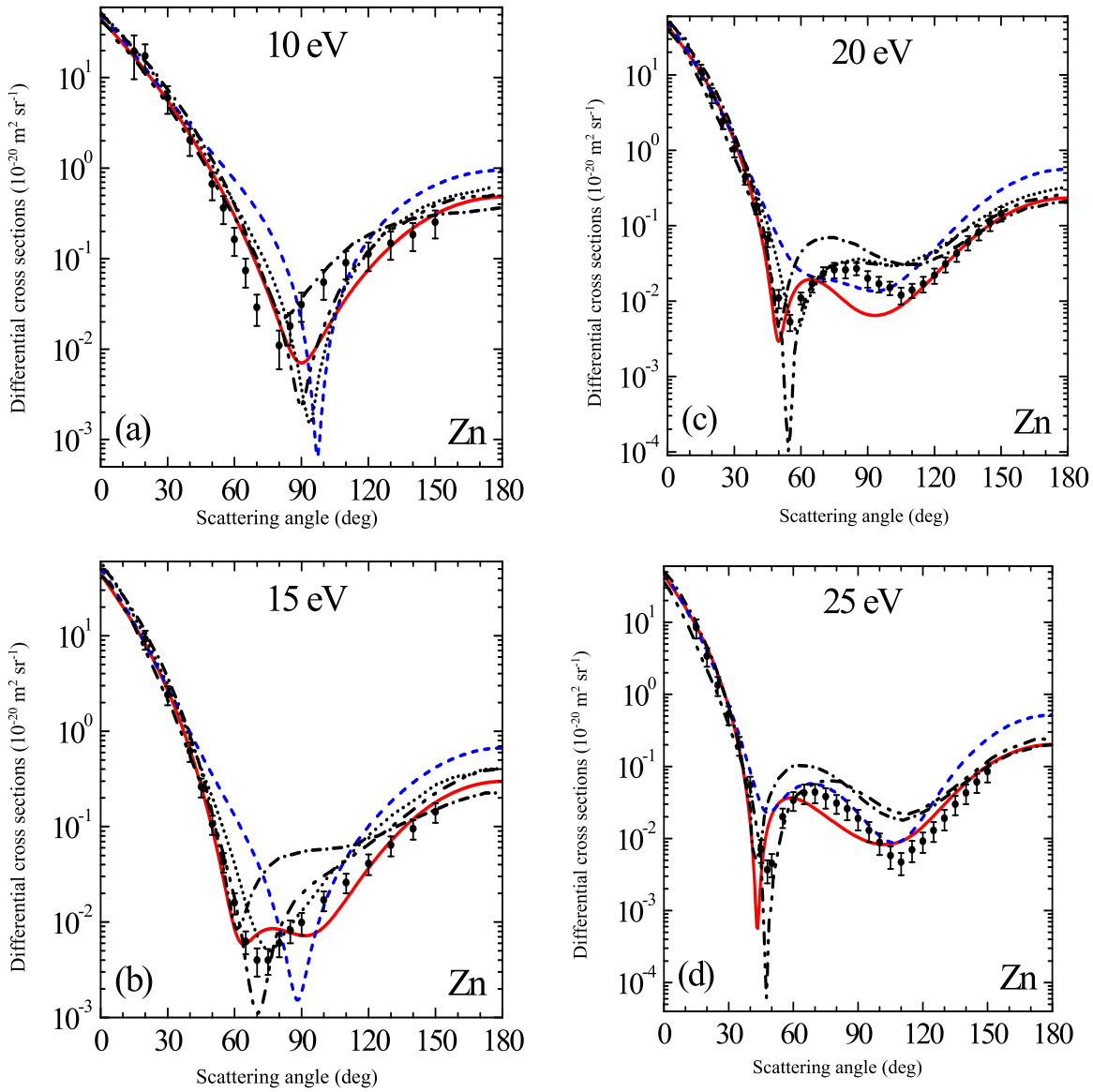

Fig. 5. Differential cross sections (in units of 10^{-20} m^2 sr^{-1}) for e^- + Zn elastic scattering at collision energies of 10(a), 15(b), 20(c) and 25(d) eV. Our present results: red solid lines – RSEPA calculations with absorption potential VaMc; blue dashed lines – RSEP calculations. Other theoretical data (black lines): dash-dotted lines – ROP [1]; dash-dot-dotted lines – BSR-36 [2]; small dots – CCC [3]. • – experimental data [1].

$$V_{so}^{\pm}(r,E) = \zeta^{\pm}(j,\ell)\frac{\chi}{r}\frac{dV_{st}}{dr},$$
$$\text{where } \chi = \alpha^2/\left[2+\alpha^2(E-V_{st})\right], \tag{3}$$

and $\zeta^{+}(j,\ell) = \ell/2$ for $j = \ell + 1/2$, $\zeta^{-}(j,\ell) = -(\ell+1)/2$ for $j = \ell - 1/2$, while $\alpha = 1/c$ is the fine structure constant and $c = 137$ is the speed of light. The Dirac-type potential [14] is used to include scalar-relativistic corrections:

$$VRS(r,E) = -\frac{\alpha^2}{2}V_{st}^2 + \frac{\chi}{4}\frac{d^2V_{st}}{dr^2} + \frac{3\chi^2}{8}\left(\frac{dV_{st}}{dr}\right)^2. \tag{4}$$

The exchange interaction is generally described by three different approximations:

I. the free electron gas (FEG) approximation [17];
II. the Furness-McCarthy (FM) potential [18];
III. the modified FM potential (MFM) based on our methodology.

In approximation I, the non-relativistic local exchange potential is given by (see, for example, Eq.(2) in [19])

$$V_e^{FEG}(r,E) = -\frac{k_F(r)}{\pi}\left(1+\frac{1-\kappa^2}{2\kappa}\ln\left|\frac{1+\kappa}{1-\kappa}\right|\right), \tag{5}$$

where $k_F(r) = [3\pi^2\rho(r)]^{1/3}$, $\kappa(r,E) = k_s(r,E)/k_F(r)$, $[k_s(r,E)]^2 = k^2 + V(r, k^2/2)$, $k^2 = 2E$. The $V(r,k^2/2)$ potential is used in the form of $V(r,k^2/2) = [k_F(r)]^2 + 2I/[1 + (kr)^2/2]$, where I is the ionization energy. The ionization energy for zinc atom is $I = 9.3943$ eV [20].

In approximation II, the Furness-McCarthy (FM) semiclassical exchange (MSCE) potential is used (see the corresponding expressions in Ref(s). [18,21–23]):

$$V_e^{FM}(r,E) = \frac{1}{2}[E - V_{st}(r)] - \frac{1}{2}\left\{[E-V_{st}(r)]^2 + 4\pi\rho(r)\right\}^{1/2}. \tag{6}$$

In the last approximation III, the FM semiclassical exchange potential (6) is modified by introducing a polarization potential $V_p(r)$:

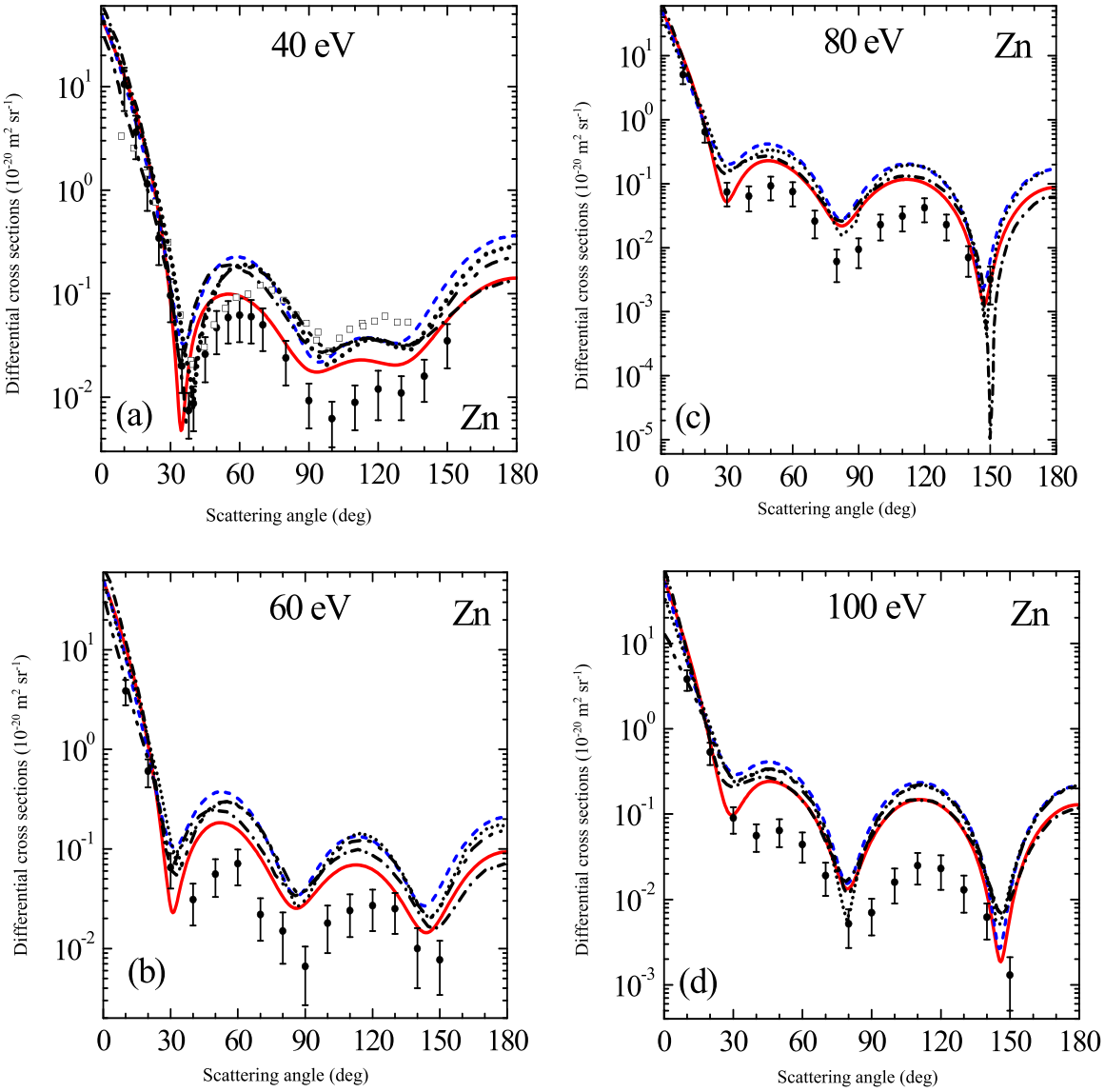

Fig. 6. Same as Fig. 5, but for collision energies of 40(a), 60(b), 80(c) and 100(d) eV. • – experimental data [1,37].

$$V_e^{MFM}(r,E) = \frac{1}{2}\left[E - V_{st}(r) - V_p(r)\right] - \frac{1}{2}\left\{\left[E - V_{st}(r) - V_p(r)\right]^2 + 4\pi\rho(r)\right\}^{1/2}. \quad (7)$$

At low energies this potential is less attractive from intermediate distances. Consequently, $|V_e^{MFM}(r,E)| < |V_e^{FM}(r,E)|$ at 0.01 eV energy from ~2 up to 15 a_0, while at 0.1 eV – from ~2.5–11 a_0 and at larger distances they are equal. This behavior is affecting the features of electron scattering at low collision energies, in the shape-resonance region. For atoms with higher dipole polarizability $\alpha_d(0)$ the effects arising from the polarization potential is obviously larger compared to atoms with lower $\alpha_d(0)$. The FM and MSCE exchange potentials are based on the Hatree-Fock theory for the scattered electron. Since the electron is scattered by a non-uniform, anisotropic potential of the target, the polarization component should be treated in the local exchange potential. It is worth to note about a modified MSCE, which was introduced by the authors of Ref. [24]:

$$V_e^{\mathrm{MSCE}}(r,E) = \frac{1}{2}\left\{E - V_{\mathrm{st}}(r) + \frac{3}{10}\left[3\pi^2\rho(r)\right]^{2/3}\right\} - \frac{1}{2}\left\{\left[E - V_{\mathrm{st}}(r) + \frac{3}{10}\left(3\pi^2\rho(r)\right)^{2/3}\right]^2 + 4\pi\rho(r)\right\}^{1/2}. \quad (8)$$

This exchange potential also can be changed as it is proposed in Eq. (7). The potentials defined by Eqs. (6) and (8) refer to the static-exchange approximation, while the inclusion of the potential defined by Eq. (7) describes the electron scattering process in the static-exchange-polarization (SEP) approximation.

It is physically acceptable to use the local correlation-polarization potential within the non-uniform electron gas model [25,26], in the role of a polarization potential $V_p(r)$. We apply the local density approximation of DFT along with a parameter-free expression for the correlation-polarization potential, which are unique for arbitrary interatomic distances [19,27]. The polarization potential consists of two parts, one of them describes this effect for short-range (SR) distances (i. e. in the inner region of the target atom), while the second is for the long-range (LR) asymptotic distances:

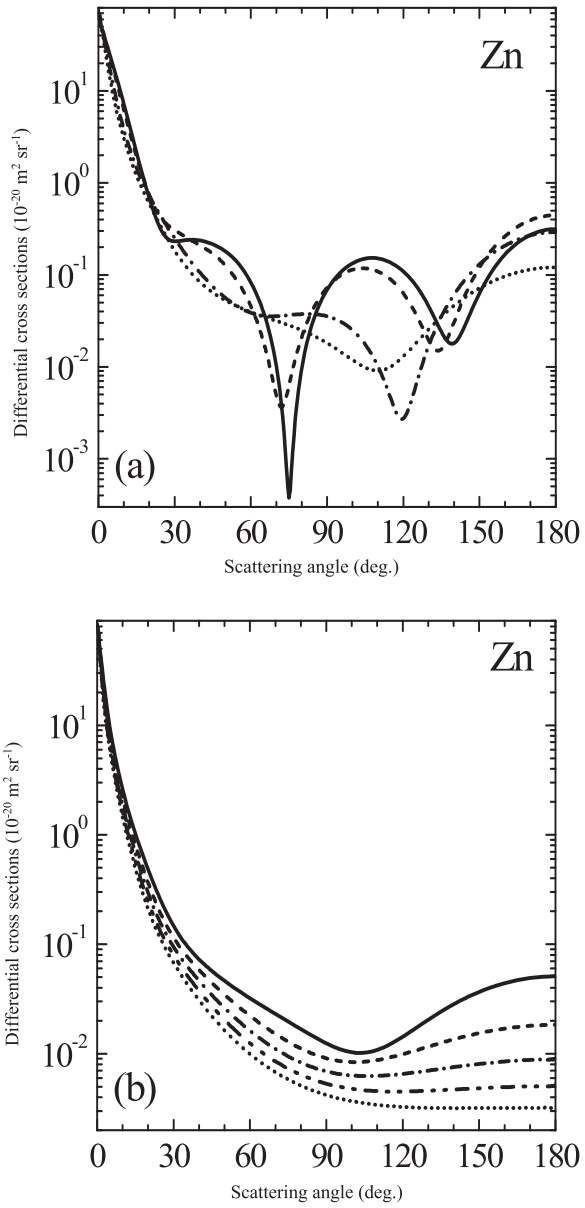

Fig. 7. Differential cross sections (in units of 10^{-20} m^2 sr^{-1}) for e^- + Zn elastic scattering at collision energies of: (a) – 150 (solid), 200 (dashed), 450 (dash-dotted) and 700 eV (dotted); (b) – 1000 (solid), 1500 (dashed), 2000 (dash-dotted), 2500 (dash-dot-dotted), 3000 eV (dotted) lines. The data are calculated using the RSEPA-approximation with the *VaMc* absorption potential.

Table 3
The energy E_c (eV) and angular θ_c (deg) positions for the critical minima in the DCSs of e^- + Zn elastic scattering, computed in the RSEP and RSEPA approximations with the VaMc absorption potential.

RSEP			RSEPA		
E_c (eV)	θ_c (deg)	DCS_{min} (10^{-20} m^2/sr)	E_c (eV)	θ_c (deg)	DCS_{min} (10^{-20} m^2/sr)
8.17	100.73	5.055(−4)*	6.63	102.34	4.683(−4)
12.57	92.42	3.053(−4)	28.24	40.47	5.892(−5)
88.80	146.47	7.433(−6)	88.47	147.02	4.670(−6)
156.64	74.49	2.927(−5)	160.71	74.32	2.121(−5)
347.24	124.14	1.546(−5)	347.53	124.11	1.319(−5)

* 5.055(-4) ≡ 5.055×10^{-4}

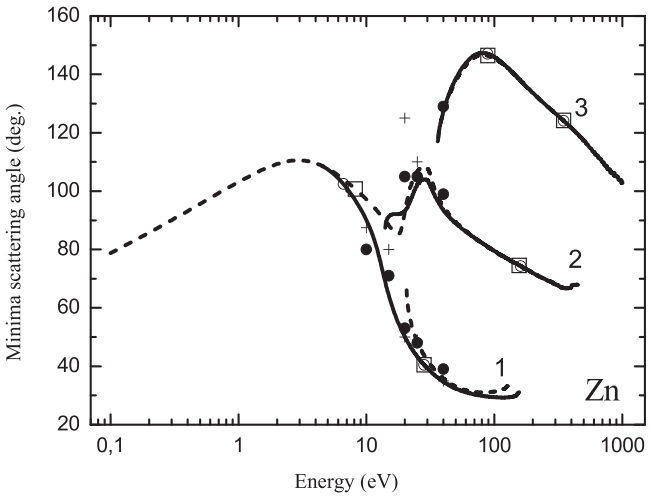

Fig. 8. Energy dependence of the angular minima positions along the DCSs of e^-+Zn elastic scattering and the corresponding critical minima. Our results with the $V_e^{MFM}(r,E)$ potential are shown for low-angle (curve 1), intermediate-angle (curves 2) and high-angle (curve 3) minima. Legend: solid line – RSEPA, dashed line – RSEP. The corresponding critical minima: ○ – RSEPA, □ – RSEP. Experiments: • – [1]; + – [38].

$$V_p(r) = \begin{cases} V_p^{SR}(r) \ , & r \le r_c \\ V_p^{LR}(r) \ , & r > r_c \end{cases} . \tag{9}$$

In the case of the zinc atom the potential $V_p^{SR}(r)$ is used in the spin-unpolarized approximation, as described in Ref. [27]:

$$V_p^{SR}(r) = \varepsilon_c(r_s) - \frac{r_s}{3}\frac{d\varepsilon_c}{dr_s} . \tag{10}$$

The correlation energy density $\varepsilon_c(r_s)$ is equal to the paramagnetic electron gas density $\varepsilon_c^P(r_s)$ and is determined as Eq. (A.4) in [27] shows. To calculate the derivative in Eq. (10) we have used the method proposed by Eq. (A.5) in [27].

The long-range part of the polarization potential has a well-known form, which is determined by the dipole static polarizability $\alpha_d(0)$:

$$V_p^{LR}(r) = -\ \alpha_d(0) \Big/ 2r^4 . \tag{11}$$

These two parts of the polarization potential (V_p^{SR} and V_p^{LR}) first cross each other at $r_c = 5.6574\ a_0$. The dipole polarizability value for the *Zn* atom is $\alpha_d(0) = 38.640\ a_0^3$, it was calculated in the local approximation of time-dependent DFT [19,28].

The phenomenological McCarthy-type absorption potential [29,30] was used in Eq. (1) as an imaginary term in the complex OP, and is defined by:

$$VaMc(r,E) = -W(E)\ r^2\ \rho_H(r)\ \big/[T_{loc}(r,E)]^2 . \tag{12}$$

The local kinetic energy is: $T_{loc} = E - V_{st} - V_e - V_p - VRS$. We used the density of the valence $4s^2$-subshell of the Zn atom ($\rho_{4s}(r)$) as the electron density of the highest filled electron shell, $\rho_H(r)$. The empirical parameter $W(E)$ was derived from inelastic scattering cross sections calculated by the Staszewska-type non-empirical absorption potential [30] in the quasi-free electron scattering model:

$$Vaf2(r,E) = -\nu_{loc}(r,E)\ \rho(r)\ \bar{\sigma}_b(r,E)/2 . \tag{13}$$

Here the local electron velocity is $\nu_{loc} = [2T_{loc}]^{1/2}$ and, contrary to [30], it includes the polarization $V_p(r)$ and $VRS(r,E)$ potentials. The average binary collision cross section $\bar{\sigma}_b(r,E)$ depends on the choice of expressions for the $\alpha(r,E)$ and $\beta(r,E)$ parameters [30]. The absorption potential Version 2 in [30] is defined by the following parameters:

Table 4
Calculated total polarization points (S=±1) for e^- + Zn elastic scattering in the RSEP- and RSEPA-approximations with V_e^{MFM} exchange and VaMc absorption potentials. The energy (–/+)ΔE and angular widths (+/–)$\Delta\theta$ are the limits for the energy and angular vicinities, where $S \geq |0.9|$.

RSEP					RSEPA				
$S(\theta)$	E (eV)	θ (deg)	(-/+)ΔE (eV)	(+/-)$\Delta\theta$ (deg)	$S(\theta)$	E (eV)	θ (deg)	(-/+)ΔE (eV)	(+/-)$\Delta\theta$ (deg)
CM [8.17 eV, 100.73°]					CM [6.63 eV, 102.34°]				
-0.9	6.85	104.21			-0.9	6.13	104.71		
–1	7.28	103.20	-0.43/+0.37	+1.01/-0.73	–1	6.33	103.97	-0.20/+0.14	+0.74/-0.41
-0.9	7.65	102.47			-0.9	6.47	103.56		
+0.9	8.66	99.12			+0.91	6.75	101.27		
+1	10.01	96.61	-1.35/+1.41	+2.51/-2.58	+1	6.91	100.78	-0.16/+0.24	+0.49/-0.90
+0.9	11.42	94.03			+0.9	7.15	99.88		
CM [12.57 eV, 92.42°]					CM [28.24 eV, 40.47°]				
+0.9	8.66	99.12			+0.9	26.32	42.12		
+1	10.01	96.61	-1.35/+1.41	+2.51/-2.58	+1	27.06	41.48	-0.74/+0.50	+0.64/-0.39
+0.9	11.42	94.03			+0.9	27.56	41.09		
-0.9	13.31	91.40	-		-0.9	28.79	39.97		
–1	13.76	90.52	-0.45/+0.66	+0.88/-1.23	–1	29.24	39.67	0.45/+0.67	+0.30/-0.46
-0.9	14.42	89.29			-0.9	29.91	39.21		
CM [88.80 eV, 146.47°]					CM [88.47 eV, 147.02°]				
+0.9	88.13	146.61			+0.9	87.82	147.18		
+1	88.44	146.58	-0.31/+0.21	+0.03/-0	+1	88.11	147.15	-0.29/+0.22	+0.03/-0
+0.9	88.65	146.58			+0.9	88.33	147.15		
-0.9	88.97	146.35			-0.9	88.62	146.90		
–1	89.19	146.35	-0.22/+0.31	+0/-0.03	–1	88.78	146.90	-0.16/+0.31	+0/-0.03
-0.9	89.50	146.32			-0.9	89.09	146.87		
CM [156.64 eV, 74.49°]					CM [160.71 eV, 74.32°]				
+0.9	153.85	74.44			+0.9	157.95	74.27		
+1	155.39	74.36	-1.54/+1.19	+0.08/-0.10	+1	159.39	74.20	-1.44/+1.15	+0.07/-0.10
+0.9	156.58	74.26			+0.9	160.54	74.10		
-0.9	156.82	74.71			-0.9	160.86	74.54		
–1	158.07	74.60	-1.25/+1.60	+0.11/-0.08	–1	162.04	74.44	-1.18/+1.52	+0.10/-0.08
-0.9	159.67	74.52			-0.9	163.56	74.36		
CM [347.24 eV, 124.14°]					CM [347.53 eV, 124.11°]				
-0.9	342.8	124.64			-0.9	342.9	124.62		
–1	345.7	124.47	-2.9/+2.5	+0.17/-0.09	–1	345.8	124.45	-2.9/+2.6	+0.17/-0.10
-0.9	348.2	124.38			-0.9	348.4	124.35		
+0.9	346.5	123.90			+0.9	346.6	123.87		
+1	348.9	123.81	-2.4/+2.9	+0.09/-0.18	+1	349.2	123.77	-2.6/+2.9	+0.10/-0.18
+0.9	351.8	123.63			+0.9	352.1	123.59		

$\alpha = k_F^2 + \Delta - 2(V_{st} + V_e + VRS)$ and $\beta = \alpha$. The Fermi-momentum of the target atom is expressed from the total electron density as $k_F(r) = [3\pi^2\rho(r)]^{1/3}$. The energy of the first inelastic threshold is Δ= 4.0061 eV, which corresponds to the ^{3}P term. We calculated its energy in the local spin-density DFT approximation [19], and our result agrees well with the data from the literature (Δ=4.0297 eV [20]).

At $E < \Delta$ the absorption potentials are equal to zero by definition. In addition, these potentials are zero at small distances as well. Thus, in the *Vaf*2 potential at small distances the cross section tends to zero ($\overline{\sigma}_b(r, E)$= 0), when $k^2 < \alpha + \beta - k_F^2$ [30]. The *VaMc* potential of Eq. (12) at small distances is negligible as compared to the real part of the OP (see Eq. (1)). For instance, at E = 10 eV and $r = 0.01\ a_0$ the real potential is V_R= –4.18·10^3 (a.u.), whereas the imaginary part is V_A= –2.64·10^{-11} (a.u.). Therefore, for $r \leq 0.01\ a_0$ we assume that $VaMc = 0$.

Using the real potential $V_R^{\pm}(r,E)$ (see Eq. (2)) we can compute the real, while by the complex OP $V_{opt}^{\pm}(r,E)$ (see Eq. (1)) – the complex partial phase shifts $\delta_\ell^{\pm}(E) = \varepsilon_\ell^{\pm}(E) + i\xi_\ell^{\pm}(E)$. The variable phase method [31,32] is used to calculate the scattering phase shifts. By this method, the absolute phase shifts are obtained from the asymptotes of the phase functions $\varepsilon_\ell^{\pm}(r,E)$ and $\eta_\ell^{\pm}(r,E)$:

$$\varepsilon_\ell^{\pm}(E) = \lim_{r\to\infty}\varepsilon_\ell^{\pm}(r,E)\ ,$$

$$\xi_\ell^{\pm}(E) = -\frac{1}{2}\ln\left[\lim_{r\to\infty}\eta_\ell^{\pm}(r,E)\right].$$

These functions obey a system of two bound, first-order non-linear differential equations. The behavior of potential $V_R^{\pm}$ Eq. (2) at low distances $r \leq r_0$ depend on the chosen boundary conditions:

$$V_R^{\pm}(r) \approx V_0 \cdot r^p\left[1 + A \cdot r^s\right],\ p > -2,\ s > 0.$$

Distance r_0 for heavy atoms is limited by the condition that the Coulomb-behavior of the static potential could be not valid at the distances $r < Z/c^2$ [33]. For example, for the Zn atom in the *s*-wave case we apply a value of $r_0 = 0.00951\ a_0$. Thus, the initial value of the phase function $\varepsilon_\ell^{\pm}(E,r)$ is determined according to expression (2.8) from Ref. [32]. The initial value for the second phase function is $\eta_\ell^{\pm}(E,r) = 1$. The numerical method for obtaining the partial phase shifts is the same as we have shown in our previous works, see, for example, [19,27].

For each collision energy E, the phases δ_ℓ^+ and δ_ℓ^- were calculated for orbital momentum value $\ell = L_1$, for which $\left|\varepsilon_\ell^+ - \varepsilon_\ell^-\right| < 0.005\%$ and $\left|\xi_\ell^+ - \xi_\ell^-\right| < 0.005\%$. For $\ell > L_1$ we assume that $\delta_\ell^+ = \delta_\ell^-$. For example, for collision energies of 10 and 3000 eV we obtain $L_1 = 4$ and $L_1 = 68$, respectively. The maximum number of the complex phase shifts are calculated using the phase equations, determined from two conditions. First, for a given energy and orbital angular momentum $\ell = L_2$ the imaginary part of the phase shift ξ_ℓ must be small enough to be considered in the denominator $\exp(2\xi_\ell)$ in the partial-wave expansions of the scattering amplitudes $f(E,\theta)$ and $g(E,\theta)$ (see Eqs. (15) and (16)) are to be equal to 1 when taking into account the DCS calculation accuracy. We assume that the values $\xi_\ell < 10^{-4}$ *rad* satisfy quite well this

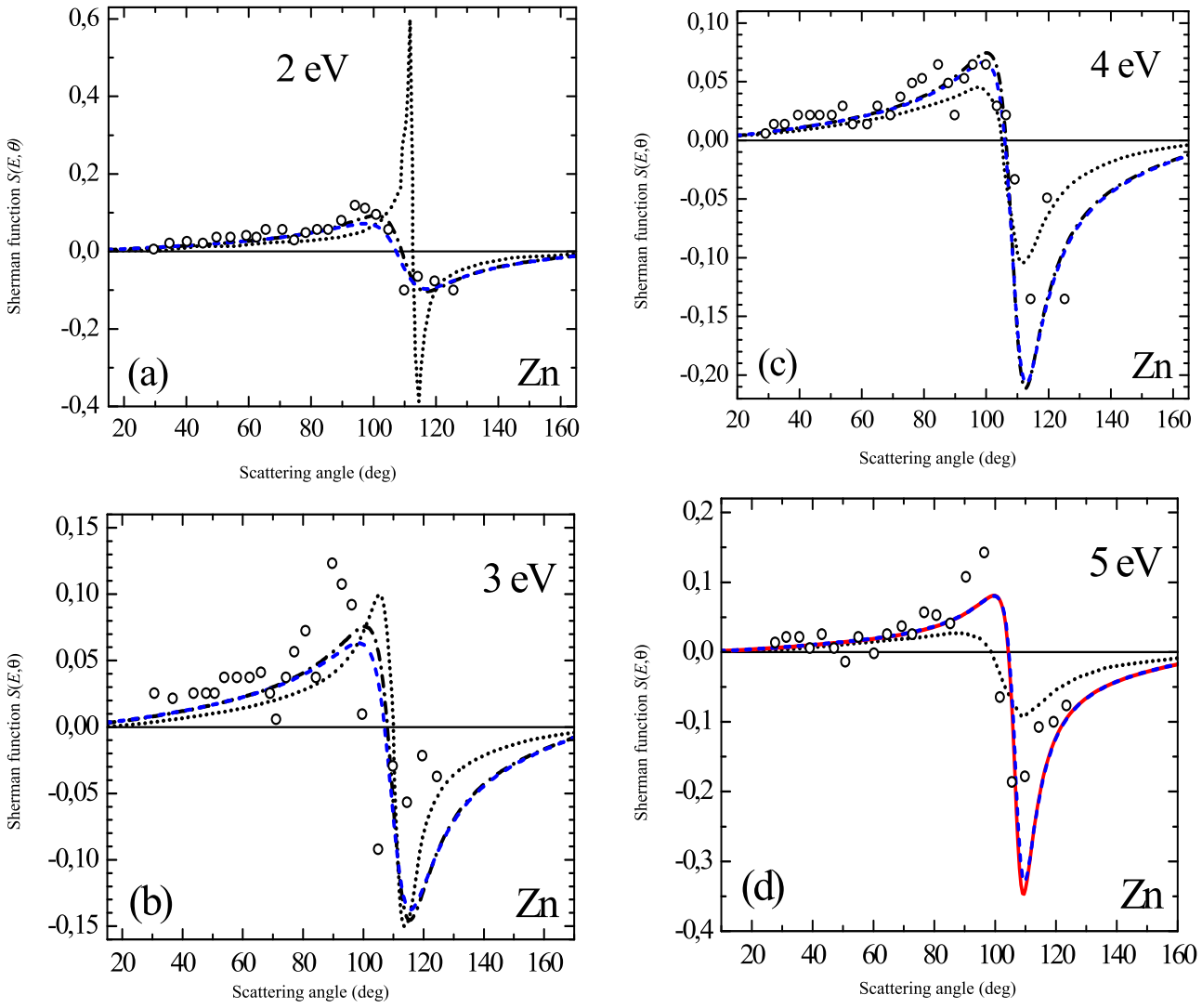

Fig. 9. Angular dependence of the Sherman function $S(E,\theta)$ as compared with the available experimental data [39] (open circles). Our calculations are: red solid line – RSEPA, blue dashed line – RSEP with $V_e^{MFM}(r,E)$ potential, black dash-dotted line – RSEP with $V_e^{FM}(r,E)$. The collision energies on the subplots are: 2 eV (a); 3 eV (b); 4 eV (c); 5 eV (d); 6 eV (e); 9 eV (f);11 eV (g) and 14 eV (h). Black dotted line – theoretical data from Ref. [40].

requirement. Second, for $\ell = L_2$, the difference between the real part of the phase shift ε_ℓ and the asymptotic value of the phase shift δ_ℓ^{as}, $|\varepsilon_\ell - \delta_\ell^{as}|$ must be less than $|\varepsilon_{\ell-1} - \delta_{\ell-1}^{as}|$ for $\ell - 1$. The phase shift δ_ℓ^{as} is calculated by the well-known formula [34]:

$$\mathrm{tg}\delta_\ell^{as} = \frac{\pi\cdot\alpha_d(0)\cdot k^2}{(2\ell+3)\cdot(2\ell+1)\cdot(2\ell-1)} \,. \tag{14}$$

At different E, the values of L_2 are different as well. For instance, at 10 and 3000 eV we found $L_2 = 10$ and $L_2 = 96$, respectively, and the corresponding phase shift values are (in radians): $\delta_{10}(10) = 9.68\cdot10^{-3} + i\ 6.34\cdot10^{-6}$ and $\delta_{96}(3000) = 3.70\cdot10^{-3} + i\ 9.81\cdot10^{-5}$. For $\ell > L_2$ we assume that $\varepsilon_\ell = \delta_\ell^{as}$ and $\xi_\ell = 0$. Since in the RSEP-approximation $\delta_\ell^{\pm}(E) \equiv \varepsilon_\ell^{\pm}(E)$, the values of L_1 and L_2 are determined from the same conditions, but for ε_ℓ. The contribution from 300 partial waves was taken into account in the calculation of the amplitude $f(E,\theta)$.

Once the phase shifts $\delta_\ell^{\pm}(E) = \varepsilon_\ell^{\pm}(E) + i\xi_\ell^{\pm}(E)$ are known, one may find the direct scattering amplitude:

$$f(E,\theta) = \frac{1}{2ik}\sum_{\ell=0}^{\infty}\left\{(\ell+1)\left[\frac{\exp(2i\varepsilon_\ell^{+})}{\exp(2\xi_\ell^{+})} - 1\right] + \ell\left[\frac{\exp(2i\varepsilon_\ell^{-})}{\exp(2\xi_\ell^{-})} - 1\right]\right\} P_\ell(\cos\theta)\,, \tag{15}$$

and the spin-flip scattering amplitude:

$$g(E,\theta) = \frac{1}{2ik}\sum_{\ell=1}^{\infty}\left[\frac{\exp(2i\varepsilon_\ell^{-})}{\exp(2\xi_\ell^{-})} - \frac{\exp(2i\varepsilon_\ell^{+})}{\exp(2\xi_\ell^{+})}\right] P_\ell^1(\cos\theta)\,, \tag{16}$$

as well as the cross sections, in particular the differential elastic scattering cross section:

$$\frac{d\sigma_{e\ell}(E,\theta)}{d\Omega} = |f(E,\theta)|^2 + |g(E,\theta)|^2\,, \tag{17}$$

the integral elastic scattering cross section:

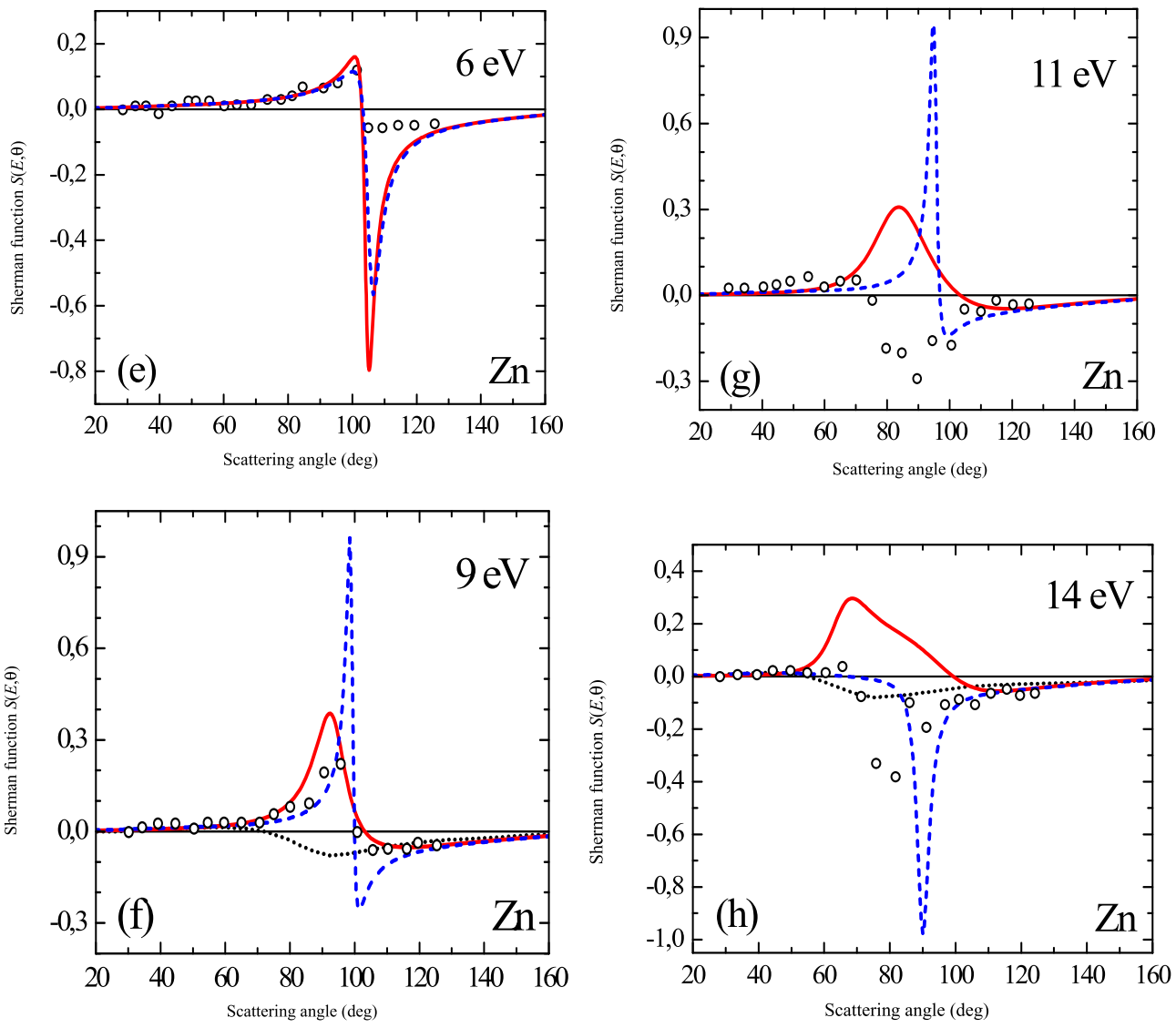

Fig. 9. (*continued*).

$$\sigma_{el}(E) = \frac{\pi}{k^2}\sum_{\ell}\{(\ell+1)\exp(-2\xi_{\ell}^{+})\ [\cosh 2\xi_{\ell}^{+} - \cos 2\varepsilon_{\ell}^{+}] + \ell\exp(-2\xi_{\ell}^{-})\ [\cosh 2\xi_{\ell}^{-} - \cos 2\varepsilon_{\ell}^{-}]\}\,, \tag{18}$$

the absorption cross section (inelastic scattering cross section):

$$\sigma_{abs}(E) = \frac{\pi}{k^2}\sum_{\ell}\{\ (\ell+1)\ [1-\exp(-4\xi_{\ell}^{+})] + \ell\ [1-\exp(-4\xi_{\ell}^{-})]\ \}, \tag{19}$$

the momentum-transfer cross section:

$$\sigma_{mom}(E) = 2\pi\int_0^{\pi}(1-\cos\theta)\cdot\sin\theta\ \frac{d\sigma(E,\theta)}{d\Omega}\ d\theta, \tag{20}$$

the viscosity cross section:

$$\sigma_{vis}(E) = 2\pi\int_0^{\pi}\sin^3\theta\ \frac{d\sigma(E,\theta)}{d\Omega}\ d\theta\,, \tag{21}$$

and the spin-polarization parameter – the so-called Sherman $S(E,\theta)$ function [15]:

$$S(E,\theta) = i\frac{f\cdot g* - f*\cdot g}{|f|^2+|g|^2}\,. \tag{22}$$

The total scattering cross section is determined then as a sum of the elastic and absorption cross sections, i.e.

$$\sigma_{tot}(E) = \sigma_{el}(E) + \sigma_{abs}(E)\,. \tag{23}$$

3. Results and discussion

The calculations have been performed in two approaches of the OP model – first, without taking into account the absorption effects (RSEP), and second, with absorption included (RSEPA). In the latter case the *VaMc* absorption potential has been used (see Eq. (12)), where the $W(E)$ parameter is calculated from as Vaf2 in Eq. (13).

3.1. Low-energy integral cross sections

In electron-atom scattering processes it is very important to accurately describe the behavior of the integral cross sections at low energies, especially below 1 eV, where a strong P-wave shape resonance is present in the case of e^- + Zn scattering. Fig. 1 shows the energy dependence of the P-wave partial phase shifts for $j = 1/2$ and $j = 3/2$,

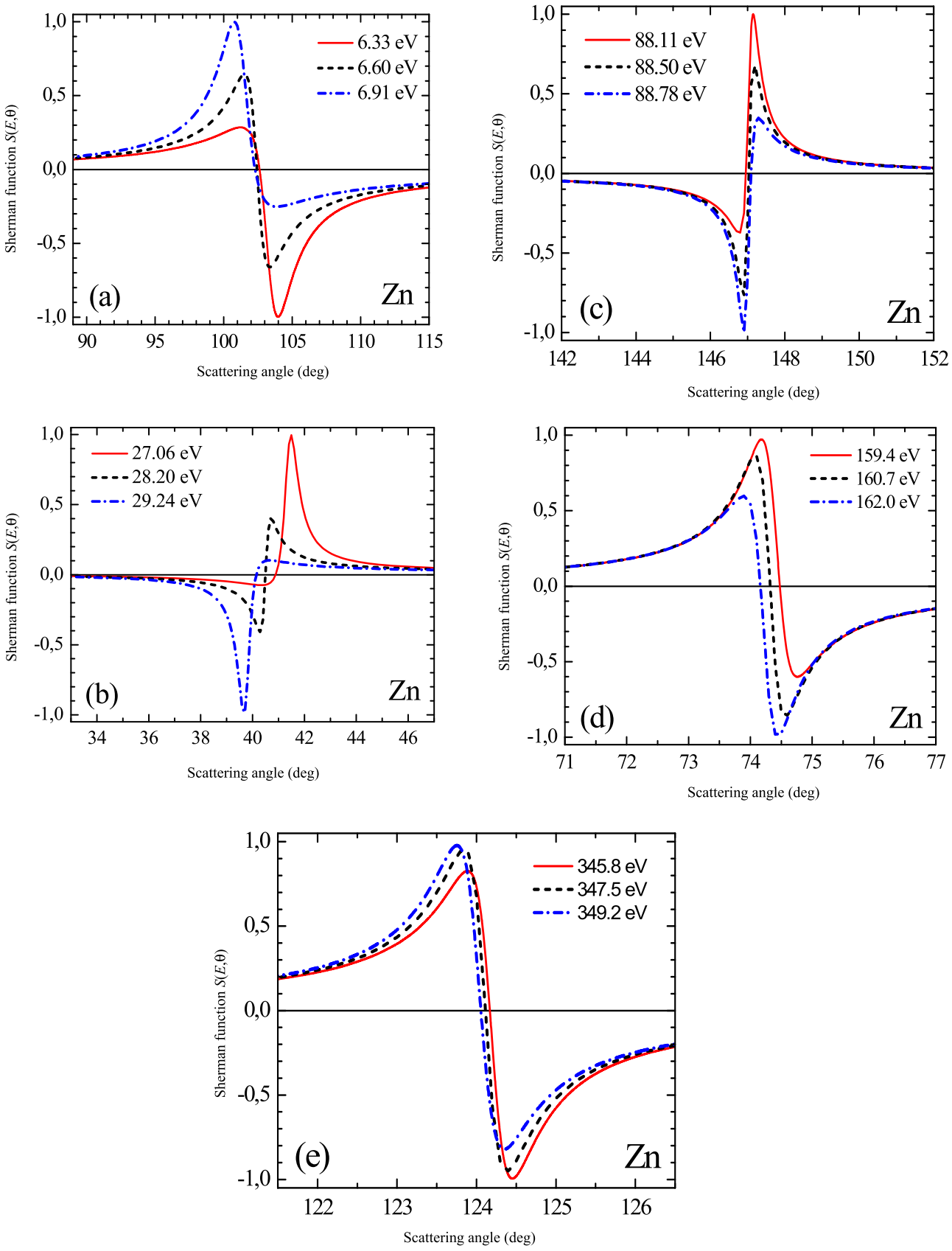

Fig. 10. Angular dependence of the Sherman function $S(E,\theta)$ at the total polarization points and at critical minima energies (RSEPA calculations with VaMc absorption potential).

calculated by the $V_e^{MFM}(r,E)$ exchange potential (see Eq. (7)). At low energies a strong peak is observed towards $\pi/2$ radian. By differentiating over the energies of the phase shifts, we obtain the following *P*-resonance parameters (energy E_r and width Γ): for $j = 1/2$ – 0.2 eV, 0.356 eV; for $j = 3/2$ – 0.19 eV, 0.309 eV (see Table 1. for more details).

Fig. 2 shows the calculated *P*-wave partial (elastic) cross sections $\sigma(E) = \sigma_{3/2}(E) + \sigma_{1/2}(E)$. These cross sections have a maximum at $\sigma_{P_{max}} = 4.39157{\cdot}10^{-18}\text{m}^2$ at ~0.28 eV collision energy. The total integral cross sections also have their maximum here, which equals to $\sigma_{max} = 4.56671{\cdot}10^{-18}\text{m}^2$. As a comparison, the authors of Ref. [1] calculated the following energy positions for this maximum: 0.4 eV and 0.28–0.35 eV, using the NOP and ROP optical potential models, respectively. Earlier, this energy was found to be equal to 0.71 eV by a 49-state BSR-method in work [2]. Our cross section at the maximum are in a very good agreement with that of found by the ROP-method in Ref. [1], and about two times lower compared to the data from Ref. [2] (see also Fig. 4a-b). Table 1 gives the particular energies at which the low-energy maximum in the elastic integral cross sections have been measured [35] or calculated [1,2].

It is worth to mention that the integral cross sections calculated by the OP method using the ELSEPA scattering code gives the following value at the maximum: $1.54664{\cdot}10^{-18}$ m^2 at 0.3 eV. Here, the experimental value was used for the static dipole polarizability, which is 47.91 a_0^3 in Ref. [36], and is slightly larger than the value we calculated, 38.640 a_0^3. As one can see, the σ_{max} value computed by the ELSEPA code is about 3 times smaller compared to our RSEP results, however the energy positions for this maximum agree very well (see Fig. 4b. below).

3.2. Integral cross sections

Fig. 3 shows the absorption integral cross sections $\sigma_{abs}(E)$ (see Eq. (19)) calculated using the absorption potential of VaMc (Eq. (12)) and the recommended inelastic cross sections $\sigma_{inel}(E)$ [4] for e^- + Zn scattering. The energy-dependent values of the $W(E)$ parameter involved in the absorption potential (12) are presented in Table 2. The inelastic cross sections were calculated as a difference of $\sigma_{inel} = \sigma_{tot} - \sigma_{el}$, where σ_{tot} is the total (23) and σ_{el} is the elastic (18) cross section. As one can see in Fig. 3, our cross section reach the maximum earlier as compared to Ref. [4].

Fig. 4 compares our integral cross sections with the corresponding experimental [1], theoretical [1,2] and recommended data [4]. The subplots 4a and 4b shows the total $\sigma_{tot}(E)$ and elastic $\sigma_{el}(E)$ cross sections, respectively, while Figs. 4c and 4d presents the momentum transfer $\sigma_{mom}(E)$ (20) and viscosity $\sigma_{vis}(E)$ (21) integral cross sections. Our data agree well with the recommended values in Ref. [4] starting already from 1 eV. Our elastic integral cross sections $\sigma_{el}(E)$ are very close to those computed by the ROP model [1] (the cross sections from the NOP model in Ref. [1] continue this behavior, but are somewhat smaller than the corresponding ROP-values). At collision energies between 1 and 10 eV all the cross sections from Ref. [1] agree with the corresponding data calculated in Ref. [2]. The cross sections computed by the CCC method in Ref. [3] well compare with the NOP-data from Ref. [1] between 10 and 100 eV. At energies 60, 80 and 100 eV all the $\sigma_{el}(E)$ cross sections are close to the corresponding experimental data.

The experimental integral cross section of elastic scattering at 40 eV in Ref. [37] equals to $2.1{\cdot}10^{-20}$ m^2. It was measured within a factor of 2 accuracy. At the same energy, the measurements carried out by the authors of [1] found this values to be $(4.27 \pm 1.49){\cdot}10^{-20}$ m^2. The corresponding value from our calculations shows $4.485{\cdot}10^{-20}$ m^2. The elastic and momentum-transfer ICSs calculated using the ELSEPA code (see Figs. 4b-4c and (18), (20)) above 1 eV well agree with our RSEP-data.

The low-energy maximum in the σ_{el}, σ_{mom} and σ_{vis} integral cross section is located in the vicinity of the *P*-wave shape resonance at 0.28, 0.26 and 0.28 eV, respectively. At larger energies (i.e. 10–300 eV) these cross sections have a rather uniform behavior with a defined secondary minimum and maximum. The inclusion of the absorption effects has significantly improved the agreement between our cross sections and the corresponding experimental data. The calculated values of the integral cross sections of the e^- + Zn scattering are given in Table S1 of the Supplementary Material.

3.3. Differential cross sections

The angular dependencies of the DCSs for elastic electron scattering by Zn atom are calculated in the RSEP- and RSEPA-approximations and are presented in Figs. 5–6 for energies, where experimental data is available in Ref. [1]. Fig. 7 shows the DCSs at high collision energies – 150, 200, 450, 700 eV and 1000, 1500, 2000, 2500, 3000 eV, where no experimental data are available at the moment. As one can see in Figs. 5–6, the number of minima along the DCSs vary with the energy: at 10 eV (Fig. 5a) only one minimum is present, while from 15 eV (Fig. 5b) up to 25 eV (Fig. 5d) a second minima can be found. By increasing the energy, we can discriminate three minima at 40 eV (Fig. 6a), 60 eV (Fig. 6b), 80 eV (Fig. 6c) and 100 eV (Fig. 6d). However, when the collision energy further increase, the DCSs reveal only two minima again – for example, at 150 eV the minimum around 30° starts to disappear, while at 200 eV (see Fig. 7a) it completely vanishes. At 450, 700, 1000, 1500 and 2000 eV only one minimum is present, which is less and less pronounced with increasing collision energy, and the DCSs become monotonous at 2500 and 3000 eV (see Fig. 7b).

As Fig. 5 reveals, our RSEPA calculations at low angles agree well with the theoretical data computed by the ROP, CCC and BSR models. As the collision energy increases, all theoretical DCSs are well-comparable with the measured data. A fairly good agreement was obtained also, when our present results are compared with the corresponding experimental data [1] at larger energies (see Fig. 6). The impact from the inclusion of the absorption effects on the angular dependencies of the DCSs are rather strong (see the DCSs from RSEP- and RSEPA-approximations in Figs. 5–6). The presence of the deep minima in the DCSs at energies of 10, 25 and 80 eV in Ref [1] could be obviously attributed to the effects of critical minima (see the CM properties in Table 3.). The calculated values of the differential cross sections of the e^- + Zn scattering are given in Tables S2-S3 of the Supplementary Material.

3.4. Critical minima in DCSs

Fig. 8 shows the energy dependence of the angular positions of the minima in the DCSs as calculated by the RSEP and RSEPA-approximations (see also Table 3). Our RSEPA calculations show that at low energies (0.1 – ~19 eV) the DCSs have minima only in the intermediate angular range, more specifically from ~80° (at 0.1 eV) up to maximum ~110° (at ~4 eV), which is further decreasing to ~83° at ~16 eV. Above 20 eV, three minima appears in the DCSs, which vanish then at a certain high-energy limits: minimum 1 at 129.5 eV, minimum 2 at 445 eV, while minimum 3 is near ~1000 eV. The inclusion of absorption effects leads to a slight shift of their positions in general and also somewhat decreases their depths.

Among all the minimal DCS values (DCSmin) we can define some of the least DCS values. For example, for the intermediate-angle minima with angular positions represented by curves 2 in Fig. 8 there are 2 such least DCS points. For the low-angle minima (curve 1) there is one least minimum. Finally, for the high-angle minima corresponding to curve 3 in Fig. 8, there are 2 such lowest DCSmin. Consequently, there are 5 deepest minima (or Critical Minima, CM) among all DCSmin, within a wide energy range (up to 300 eV). We denote the energy and angular positions of these CM as critical energy E_c and critical angle θ_c (see Table 3 for details). Note that the energies and angles of the first two low energy CMs are strongly affected by the account of absorption effects.

Our results are compared with the corresponding experimental data [8,38] in Fig. 8. In Ref. [8,9 minima have been measured along the DCS:

[10 eV, 80°], [15 eV, 71°], [20 eV, 53°], [20 eV, 105°], [25 eV, 48°], [25 eV, 105°], [40 eV, 39°], [40 eV, 99°], [40 eV, 129°]. The experimental values obtained for 39° and 99° at 40 eV in Ref. [37] are close to the corresponding data in Ref. [8]. The energy-dependence of the calculated angular positions for the DCSs minima in Ref. [6,7] in the 10–40 eV energy region are well reproduced by our calculations. The calculated DCSs [9] at energies 12.5, 25, 100 and 200 eV are characterized with the following 7 minima – 90° ($4.5{\cdot}10^{-22}$ m^2/sr); ~57° ($5.6{\cdot}10^{-22}$ m^2/sr) and ~122° ($5.6{\cdot}10^{-22}$ m^2/sr); ~82° ($1.7{\cdot}10^{-22}$ m^2/sr) and ~146° ($5.6{\cdot}10^{-23}$ m^2/sr); ~72.5° ($8.4{\cdot}10^{-23}$ m^2/sr) and 135° ($2.2{\cdot}10^{-22}$ m^2/sr), respectively.

In papers [6,7] the CM position are found to be [26.0 eV, 116°] with a DCS value of $7{\cdot}10^{-23}$ m^2/sr. The authors mention that these data agree well with the experimental values from Ref. [8] for the minimum [25.0 eV, 105°]. Based on our calculations one can see that at [25.0 eV, 105°] the DCSs have a usual minimum, while the CM is located at [28.24 eV, 40.47°] with a cross section value of $5.893{\cdot}10^{-25}$ m^2/sr (see its parameters in Table 3). One of the clear signs of a CM is the presence of the following relation between the scattering amplitudes defined by Eqs. (15)-(16): $|f(E,\theta)|^2 < |g(E,\theta)|^2$. So, in the RSEP model at 12.57 eV the CM in DCS is located at 92.42°, where $|f(E,\theta)|^2 = 1.10936{\cdot}10^{-26}\ m^2/sr$, $|g(E,\theta)|^2 = 3.04176{\cdot}10^{-24}\ m^2/sr$, while at 28 eV a simple minimum is found at 108.4°, where $|f(E,\theta)|^2 = 6.4786{\cdot}10^{-23}\ m^2/sr$, $|g(E,\theta)|^2 = 8.10707{\cdot}10^{-25}\ m^2/sr$. According to the RSEPA DCS-calculations at 28.24 eV and 40.47° the CM is characterized by $|f(E,\theta)|^2 = 8.5099{\cdot}10^{-28}\ m^2/sr$ and $|g(E,\theta)|^2 = 5.8839{\cdot}10^{-25}\ m^2/sr$, i.e. $|f(E,\theta)|^2 < |g(E,\theta)|^2$.

3.5. Spin-polarization

As mentioned above, the advantage of determining the CM positions is related to the fact, that in the vicinity of these minima the scattered electron's total spin-polarization could be determined. Table 4 presents the positions of the total polarization points, as calculated in the RSEP- and RSEPA-approximations. We have identified 10 points in the vicinity of the CMs. For each of these points, we calculated the energy (–/+)ΔE and angular (+/–)$\Delta\theta$ widths in the vicinity of strong (≥|90|%) polarization. Accordingly, the energy and angular widths at $S \geq |0.9|$ are also listed in Table 4. The ΔE and $\Delta\theta$ values non-linearly vary with energy – ΔE is increasing up to a few eV, while $\Delta\theta$ is decreasing down to a few hundredths of a degree. For the CM [88.47 eV, 147.02°] the widths are characterized by their average minimum values.

Fig. 9 presents the angular dependencies of the Sherman functions $S(E,\theta)$ Eq. (22) as calculated in the RSEP- and RSEPA-approximations and compared with the experiment of Ref. [39]. In general, a good qualitative and adequate quantitative agreement is found between our RSEPA theoretical data and the corresponding measured quantities. In Fig. 9a-d, f-h we compare our results with the theoretical data from Ref. [40], which were calculated considering the relativistic effects and exchange interactions. At 3 and 4 eV, the Sherman functions from [40] are in a good agreement with the measured values [39]. From 6 eV (Fig. 9e) up to 14 eV (Fig. 9h) the absorption effects are more pronounced. One can see in Fig. 9a-d that the difference between the $S(E,\theta)$ functions calculated with two different exchange potentials – $V_e^{FM}(r,E)$ and $V_e^{MFM}(r,E)$ – is decreasing with increasing collision energy. The strong non-linear variation of the polarization functions from ~+ 0.07 to ~− 0.35 at 5 eV and angles between 100°-110° (Fig. 9d) is due to the CM at [6.63 eV, 102.34°]. For collision energies of 11 and 14 eV (see Fig. 9g-h) the calculated Sherman functions are only in a qualitative agreement with the measurements carried out in Ref [39].

Fig. 10 shows the angular dependence of the Sherman functions (RSEPA-approximation) in the vicinity of the five critical minima. As one can see, the angular behavior of the $S(E,\theta)$ functions reach the maximum (+1) and minimum (−1) in the proximity of the CM, when the collision energy is changing from lower (solid curves) towards higher (dash-dotted curves) values. This trend in the spin-polarization clearly demonstrates the role of the CM in the differential cross sections of electron scattering.

4. Conclusion

The process of elastic electron scattering by zinc atom has been studied in a wide collision energy range (from 0.01 up to 3000 eV) within the framework of the relativistic optical potential approximation, in which the real part is parameter-free. The differential cross sections' minima and the spin-polarization effects are in the main focus of the study. Relativistic effects have been taken into account by applying a spin-orbit interaction potential, which is based on the scalar part of the relativistic Dirac potential. Our results are in a good agreement with the available experimental and theoretical data from literature.

The complex optical potential, which was used in the present calculations, is mainly determined by the total and valence electron densities of the target atom. The densities and other related properties of the zinc atom (static dipole polarizability, ionization potential, *etc.*) were calculated in the local approximation of density functional theory, including the relativistic effects. This approximation is used to describe the overall electron scattering process, which is then rather consistent with the description of the atomic properties.

A modified Furness-McCarthy exchange potential is proposed by counting for the polarization effects. This modified exchange-polarization potential allows a more accurate description of low-energy (<10 eV) electron scattering.

The behavior of the elastic integral cross sections have been studied at low energies. Its maximum is mostly due to the *P*-wave partial cross sections. The energy dependence of the partial phase shifts implies the presence of a *P*-wave shape resonance at ~0.2 eV collision energy with characteristic widths of ~0.309 ($j = 3/2$) and 0.356 ($j = 1/2$) eV.

The calculated energy dependence of the total, elastic, momentum transfer and viscosity integral cross section are characterized by a low-energy maximum (near 1 eV) and a non-linear "minimum-maximum"-type behavior in the 10–100 eV energy range. The inclusion of absorption effects implies a significant improvement in the cross sections, leading to better agreement with the corresponding experimental data. The computed integral and differential cross sections are in a good agreement with these measured data, while they are also well-comparable with other existing theoretical results. Accounting the inelastic (absorption) processes in the imaginary part of the optical potential significantly impacts the overall behavior and the amplitudes of the cross sections as well as the Sherman functions.

The total number of minima positions in the differential cross sections varies from 1 to 3 depending on the collision energy. The energy and angular positions are identified for 5 critical minima in the differential cross sections. According to our RSEPA calculations, the lowest among the critical angles θ_c is around 40.47° (at E_c=28.24 eV), while the largest is 147.02° (at E_c=88.47 eV). The minimum with the lowest critical energy is 6.63 eV, and located at θ_c= 102.34°, while the highest is found to be around 347.53 eV (at θ_c=124.11°). The differential cross section values in the critical minima are ranging from $4.7{\cdot}10^{-24}$ up to $4.7{\cdot}10^{-26}$ m^2/sr.

The Sherman functions calculated at low energies are in a good agreement with the experimental findings. In the vicinity of the critical minima, the position of 10 total polarization points were determined, where the Sherman function are $S(E,\theta) = \pm 1$. In the vicinity of the critical minima there are also some small energy and angular intervals, where the spin-polarization is large ($|S| \geq 0.9$).

The results obtained in this work demonstrate that such sensible scattering properties like the critical minima in the differential cross sections as well as the total spin-polarization points are good candidates for theoretical predictions and may serve as a probe of the different approximations. Such quantities could be targeted also by experimental

studies for elastic electrons scattering.

The authors dedicate this paper to the memory of their friend and colleague, Oleg Ivanovich Zatsarinny, who was a pioneer in development of R-matrix theories for accurate treatment of electron-atom and electron-ion scattering processes, and who passed away on 2 March, 2021, at the age of 67.

Declaration of Competing Interest

The authors declare no conflict of interest.

Data Availability

No data was used for the research described in the article.

Acknowledgements

Open access funding provided by Institute for Nuclear Research (ATOMKI) within the agreement of the Hungarian consortium EISZ and publisher Elsevier. Financial support was provided by Institute of Electron of Physics National Academy of Sciences of Ukraine to condusct this research. This work was also supported by the National Research, Development and Innovation Office (NRDIO) Research Fund (Grant No. K128621).

Appendix A. Analytical expressions and parameters used to determine the total electron density $\rho(r)$ and the static potential $V_{st}(r)$ in the case of the zinc atom

The static potential $V_{st}(r)$ and the total electron density $\rho(r)$ for the zinc atom are calculated using the following analytical expressions [16].

$$V_{st}(r) = -\frac{Z}{r}\left[\sum_{i=1}^{n} A_i \exp\left(-B_i r\right) + r\sum_{j=1}^{m} C_j \exp\left(-D_j r\right)\right] \tag{A1}$$

and

$$\rho(r) = \frac{Z}{4\pi r}\left[\sum_{i=1}^{n} A_i B_i^2 \exp(-B_i r) + \sum_{j=1}^{m} C_j D_j \left(D_j r - 2\right)\exp\left(-D_j r\right)\right], \tag{A2}$$

where Z is the charge of the nucleus of the target atom.

The number and the value of the parameters in Eq. (A2) have been found from the best approximation to the initial table for the density $\rho(r)$, calculated within the framework of local DFT. In (A1) and (A2), the number of addends in the sums is n = 3 and m = 4. The parameters A, B, C and D are defined as follows: $A_1 = 1.8797$, $A_2 = -0.8535$ and $A_3 = 1 - A_1 - A_2$ are dimensionless; $B_1 = 4.7954$, $B_2 = 37.065$, $B_3 = 84.5$, $C_1 = -12.203$, $C_2 = -18.079$, $C_3 = 0.4567$, $C_4 = 0.1865$, $D_1 = 10.737$, $D_2 = 29.284$, $D_3 = 3.0951$ and $D_4 = 1.6046$ are expressed in units of a_0^{-1}, where a_0 is the first Bohr radius of the hydrogen atom.

Appendix B. Analytical expressions and the parameter used to determine the electron density of the valence 4 *s*-subshell $\rho_{4s}(r)$ in the case of the zinc atom

The electron density of the valence 4 *s*-subshell is related to the electron orbital

$$\rho_{4s}(r) = 2\phi_{4s}^2(r) \tag{B.1}$$

The analytical expression for this orbital is given in a Slater-form:

$$\varphi_{4s}(r) = \sum_{i=1}^{4} K_i \cdot r^{M_i} \cdot exp(-N_i r)\,. \tag{B.2}$$

Parameters in Eq. (B.2) are: $K_1 = -29.652$, $K_2 = -35.035$, $K_3 = 2.5719$, $K_4 = -0.3587$; $M_1 = 1.1331$, $M_2 = 0.8715$, $M_3 = -0.01558$, $M_4 = 0.9015$; $N_1 = 8.4491$, $N_2 = 13.358$, $N_3 = 3.3074$ and $N_4 = 0.9758$. The M_i parameters are dimensionless, while N_i are expressed in a_0^{-1}. The dimension of the K_i parameters is defined by the $\rho_{4s}(r)$ density normalization.

Appendix A. Supporting information

Supplementary data associated with this article can be found in the online version at doi:10.1016/j.elspec.2023.147365.

References

[1] B.P. Marinković, R. Panajotović, D. Šević, R.P. McEachran, G. García, F. Blanco, M. J. Brunger, Phys. Rev. A 99 (2019), 062702.
[2] O. Zatsarinny, K. Bartschat, Phys. Rev. A 71 (2005), 022716.
[3] D.V. Fursa, I. Bray, R. Panajotović, D. Šević, V. Pejčev, D.M. Filipović, B. P. Marinković, Phys. Rev. A 72 (2005), 012706.
[4] R.P. McEachran, B.P. Marinković, G. García, R.D. White, P.W. Stokes, D.B. Jones, M.J. Brunger, J. Phys. Chem. Ref. Data 49 (2020), 013102.
[5] S. Chen, R.P. McEachran, A.D. Stauffer, J. Phys. B:. Mol. Opt. Phys. 41 (2008), 025201, https://doi.org/10.1088/0953-4075/41/2/025201.
[6] J.E. Sienkiewicz, S. Telega, P. Sytya, S. Fritzsche, Phys. Lett. A 293 (2002) 183–187.
[7] J.E. Sienkiewicz, S. Telega, P. Sytya, S. Fritzsche, Radiat. Phys. Chem. 68 (2003) 285–289.
[8] B. Predojević, D. Šević, R. Panajotović, V. Pejčev, D.M. Filipović, B.P. Marinković, Book of Abstracts, 20th SPIG, Belgrade, Yugoslavia, 2000, p. 35.
[9] D.B. McGarrah, A.J. Antolak, W. Williamson Jr., J. Appl. Phys. 69 (1991) 6812.
[10] W. Bühring, Z. Phys. 208 (1968) 286–298.
[11] V.I. Kelemen, E. Yu Remeta, J. Phys. B:. Mol. Opt. Phys. 45 (2012), 185202.

[12] F. Salvat, A. Jablonski, C.J. Powell, Comp. Phys. Commun. 165 (2005) 157.
[13] R. Cowan, The Theory of Atomic Structure and Spectra, University of California Press,, Berkeley, CA, 1981.
[14] L.T. Sin Fai Lam, J. Phys. B:. Mol. Phys. 15 (1982) 119–142.
[15] J. Kessler, Adv. Mol. Opt. Phys. 27 (1991) 81–163.
[16] T.G. Strand, R.A. Bonham, J. Chem. Phys. 40 (1964) 1686–1691.
[17] S. Sur, A.S. Ghosh, Ind. J. Phys. 57B (1983) 67–70.
[18] J.B. Furness, I.E. McCarthy, J. Phys. B V.6 (1973) 2280.
[19] V.I. Kelemen, E.Yu Remeta, E.P. Sabad, J. Phys. B:. Mol. Opt. Phys. 28 (1995) 1527–1546.
[20] A.A. Radzig, B.M. Smirnov, Reference Data on Atoms, Molecules, and Ions, Springer,, Berlin, 1985.
[21] M.E. Riley, D.G. Truhlar, J. Chem. Phys. V.63 (1975) 2182.
[22] R. Vanderpoorten, J. Phys. B V.8 (1975) 926.
[23] B.H. Bransden, M.R.C. McDowell, C.J. Noble, T. Scott, J. Phys. B V.9 (1976) 1301.
[24] F.A. Gianturco, S. Scialla, J. Phys. B:. Mol. Phys. 20 (1987) 3171–3189.
[25] J.K. O'Connell, N.F. Lane, Phys. Rev. A 27 (1983) 1893–1903.
[26] N.T. Padial, D.V. Norcross, Phys. Rev. A 29 (1984) 1742–1748.
[27] E.Yu. Remeta, V.I. Kelemen, J. Phys. B:. Mol. Opt. Phys. 43 (045202) (2010) 10.
[28] A. Zangwill, P. Soven, Phys. Rev. A 21 (1980) 1561–1572.
[29] I.E. McCarthy, C.J. Noble, B.A. Philips, A.D. Turnbull, Phys. Rev. A 15 (1977) 2173–2185.
[30] G. Staszewska, D.W. Schwenke, D.G. Truhlar, *Phys. Rev.* A 29 (1984) 3078–3091.
[31] F. Calogero, Variable Phase Approach to Potential Scattering, Academic, New York, 1967.
[32] V.V. Babikov. Phase Function Method in Quantum Mechanics, Third ed., Nauka) (in Russian), Moscow, 1988.
[33] V.A. Fock. Foundations of Quantum Mechanics, Second ed., Nauka) (in Russian), Moscow, 1976.
[34] P.G. Burke, Potential Scattering in Atomic Physics, Plenum, New York, 1977.
[35] P.D. Burrow, J.A. Michejda, J. Comer, J. Phys. B 9 (1976) 3225.
[36] D.R. Lide. CRC Handbook of Chemistry and Physics, 79th ed., CRC Press, Boca Raton, FL, 1999.
[37] W. Williams, D. Bozinis, Phys. Rev. A 12 (1975) 57.
[38] E.C. Childs, H.S.W. Massey, Proc. R. Soc. A 142 (1933) 509.
[39] M. Bartsch, H. Geesmann, G.F. Hanne, J. Kessler, J. Phys. B:. Mol. Opt. Phys. 25 (1992) 1511–1526. N 7.
[40] R.P. McEachran, A.D. Stauffer, J. Phys. B: Atomic Mol. Opt. Phys. 25 (1992) 1527–1532.